Supporting information

Supramolecular ionogels enable highly efficient electrochromism

Kaijian Zhou,‡[a] Liang Tang,‡[a] Guoqiang Kuang,[a] Jun Zhang,[a] Zhiyong Li,[b] Guoqiang Xing,[a] Xueao Jiang,[a] Zhanying Chen,[a] Yijie Tao,*[a] Yan Zhang,*[a] and Shiguo Zhang*[a]

[a]*College of Materials Science and Engineering, State Key Laboratory of Advanced Design and Manufacturing Technology for Vehicle, Hunan University, Changsha 410082, Hunan, China*

[b]*School of Chemistry and Chemical Engineering, Henan Normal University, Xinxiang, 453007, Henan, China*

Materials

Acetonitrile (99%), [BMIm][TFSI] (1-butyl-3-methylimidazolium bis(trifluoromethylsulfonyl)imide, 99%), DBS (1,3:2,4-dibenzylidene-d-sorbitol, 95%), 4,4'-bipyridine (98%), 1-bromoheptane (98%), LiTFSI (lithium bis(trifluoromethanesulfonyl)imide, 99.95%), ferrocene (Fc 99%), ethanol (99%), 2,4-dinitrochlorobenzene (99%), 4-cyanoaniline (98%), benzyl chloride (99%), ethyl acetate (99.5%), methanol (99.5%), acetone (99%), and xylene (99%) were sourced from Aldin, China, and utilized without further purification. ITO-coated glass

(Rsh=7.9-9.3Ω/sq) and ITO-coated PET film (Rsh=18Ω/sq) were obtained from Zhuhai Kaiwei Optoelectronic Technology Co., Ltd, China. PEDOT:PSS was acquired from Hunan Nasheng Electronic Technology Co., Ltd, China. PProDOT-C8 synthesis followed prior reports[1], and the preparation of viologen-based electrochromic materials DHV[TFSI]$_2$, CNPV[TFSI]$_2$, and MBV[TFSI] is also referenced from previous work[2], with details provided in Figure S1. Their 1H NMR spectra are displayed in Figure S2.

Instrument and characterizations

^{1}H NMR spectra were acquired using a Bruker 400 MHz instrument with TMS as a reference. Infrared (IR) spectra were recorded on a Thermo Fisher Scientific Nicolet iS50 spectrometer. The xerogel DBS-G's microstructure was examined with a Hitachi-S4800 scanning electron microscope (SEM), while the morphology was observed using an Olympus BX53MRF-S Polarizing microscope (POM). Differential scanning calorimetry (DSC) was conducted on a Mettler-Toledo DSC822e at a 10°C min^{-1} rate under nitrogen. Thermogravimetric (TG) analysis was performed on a Hitachi STA7200 system at a 10°C min^{-1} rate in argon. Rheological properties were assessed with an Anton Paar MCR 92 rheometer using a 25 mm diameter cone with a 1° angle and 0.051 mm gap. X-ray diffraction (XRD) patterns were obtained on a Rigaku MiniFlex600 diffractometer at a 10 degrees min^{-1} scan rate. Adhesion strength was evaluated on an MX-0580 tensile tester at 100 mm min^{-1}, with each test repeated five times. UV–vis spectra were captured using a Shimadzu UV-2600 spectrometer.

Electrochemical properties were analyzed with a CHI 660 Electrochemical workstation. The baseline during testing has been calibrated using blank samples. In the UV-vis spectroscopy test of PProDOT-C8-ECD, a blank device was constructed, consisting of ITO-coated glass, a PEDOT:PSS counter electrode sprayed onto the ITO glass, and supramolecular ionogels (DBS-G). After the instrument was powered on and parameters were set, baseline calibration was performed using this blank device as the reference. The UV-vis test was then carried out according to standard operational procedures. Similarly, in the UV spectrum test of viologen-ECDs, a blank device comprising two ITO-coated glasses and supramolecular ionogels was assembled. This blank device was used for baseline calibration, allowing for accurate measurement of the UV absorption characteristics of the viologen within its system. Color differences (ΔE*) were quantified using a X-rite CI64 color difference meter. Ionic conductivity was determined using a DZS-706-A multi-parameter analyzer. After powering on the ionic conductivity meter and calibrating it with a 0.1 M KCl standard solution, the DBS-G sample is heated to form a sol. The test probe of the ionic conductivity meter is then immersed into the sol for measurement. The sol is allowed to cool and solidify into a gel as the system naturally returns to ambient temperature. The ionic conductivity reading displayed on the instrument corresponds to the final measurement at room temperature.

Preparation of DBS-G

A supramolecular ionogel, referred to as DBS-G, is synthesized by heating an

ultrasonic-treated mixture of 0.05g DBS and 0.95g [BMIm][TFSI] to 120 °C, followed by cooling to ambient temperature to achieve a uniform gel.

Preparation of viologen-containing DBS-G

viologen-containing DBS-G gels, designated as DHV$[TFSI]_2$-G, were synthesized by combining 2.88g (2 mL) [BMIm][TFSI], 0.157g DBS (5 wt% based on total mass), 18.6 mg (0.05 mol/L) ferrocene and 91.5 mg (0.05 mol/L, relative to the ionic liquid concentration) viologens DHV$[TFSI]_2$. Note that since Fc balances the ionic potential in the electrochromic process of viologen molecules, an equimolar amount of Fc is added to achieve charge balance. The mixture was subjected to ultrasonication for 5 minutes, then heated to 120°C to form a homogeneous solution, which was then cooled to room temperature. Similarly, the CNPV$[TFSI]_2$-G, were synthesized by combining 2.88g(2 mL) [BMIm][TFSI], 0.157g DBS (5 wt% based on total mass), 18.6 mg (0.05 mol/L) ferrocene and 92 mg (0.05 mol/L, relative to the ionic liquid concentration) viologens CNPV$[TFSI]_2$. And the MBV[TFSI]-G, were synthesized prepared by 2.88g [BMIm][TFSI], 0.155g DBS, 18.6 mg ferrocene and 52.7 mg MBV[TFSI].

Preparation of MEA-G

The MEA-G gel was fabricated by blending 2g(50 wt%) 2-methoxyethyl acrylate (MEA), 2g(50 wt%)50 wt% BMIm][TFSI], 0.003gcrosslinker 1,6-hexanediol diacrylate (relative to the combined mass of MEA and [BMIm][TFSI]), and 0.003g photoinitiator 2,2-Diethoxyacetophenone (also relative to the combined mass of MEA

and [BMIm][TFSI]) to form a uniform solution, followed by UV light curing for 30 minutes.

Fabrication of PProDOT-C8-ECDs using DBS-G

ITO-coated glass (5×5 cm) was cleaned ultrasonically with ethanol and acetone. PProDOT-C8 (20 mg) was dissolved in xylene (10 mL), and PEDOT:PSS was mixed with ethanol in a 1:5 volume ratio for spraying onto the glass to form a film using a spray gun. The two glass pieces were assembled into a device with a 100 μm gap using double-sided tape. The DBS-G was melted in a 120°C oven, injected into the gap with a syringe, and cooled to room temperature to produce the PProDOT-C8-ECD.

Fabrication of PProDOT-C8-ECDs using MEA-G

Two ITO-coated glasses (5×5 cm), coated with PProDOT-C8 and PEDOT:PSS, were assembled into an electrochromic device using double-sided tape to maintain a 100 μm gpa. The MEA and [BMIm][TFSI] solution was injected and cured under UV light for 30 minutes to form the PProDOT-C8-ECD.

Fabrication of viologen-ECDs using viologen-containing DBS-G

Two ITO-coated glasses (5×5 cm) were combined to form a device with a 100 μm gap using double-sided tape. The EC gels DHV[TFSI]$_2$-G, CNPV[TFSI]$_2$-G, and MBV[TFSI]-G were heated in a 120°C oven until liquefied and then injected into the device gap, followed by cooling to room temperature to produce DHV[TFSI]$_2$-G-ECD,

CNPV[TFSI]$_2$-G-ECD, and MBV[TFSI]-G-ECD. For flexible ECDs, ITO-coated PET (4×4 cm) was used with a 200 μm gap, adhering to the same fabrication process.

Fabrication of DHV[TFSI]$_2$-PMMA-ECD

The traditional ionogel was synthesized using PMMA and [BMIm][TFSI] ionic liquid based on a previous literature (*Adv. Funct. Mater. 2014, 24, 2837-284*). More specifically, 1.18 g of PMMA (Mw = 200,000) was dissolved in 20 mL of THF. Then, 2.75 g of [BMIm][TFSI], 118 mg of DHV[TFSI]$_2$, and 24 mg of ferrocene were added. The mixture was stirred for 30 minutes, followed by ultrasonic treatment for 10 minutes to remove trapped air. The resulting solution was cast into a PTFE mold and left overnight at 40°C. It was then heated under vacuum at 40°C for 4 hours to eliminate the solvent, yielding the final polymer electrolyte. This polymer electrolyte was sandwiched between two ITO layers, with a gap of approximately 200 μm, to create DHV[TFSI]$_2$-PMMA-ECD.

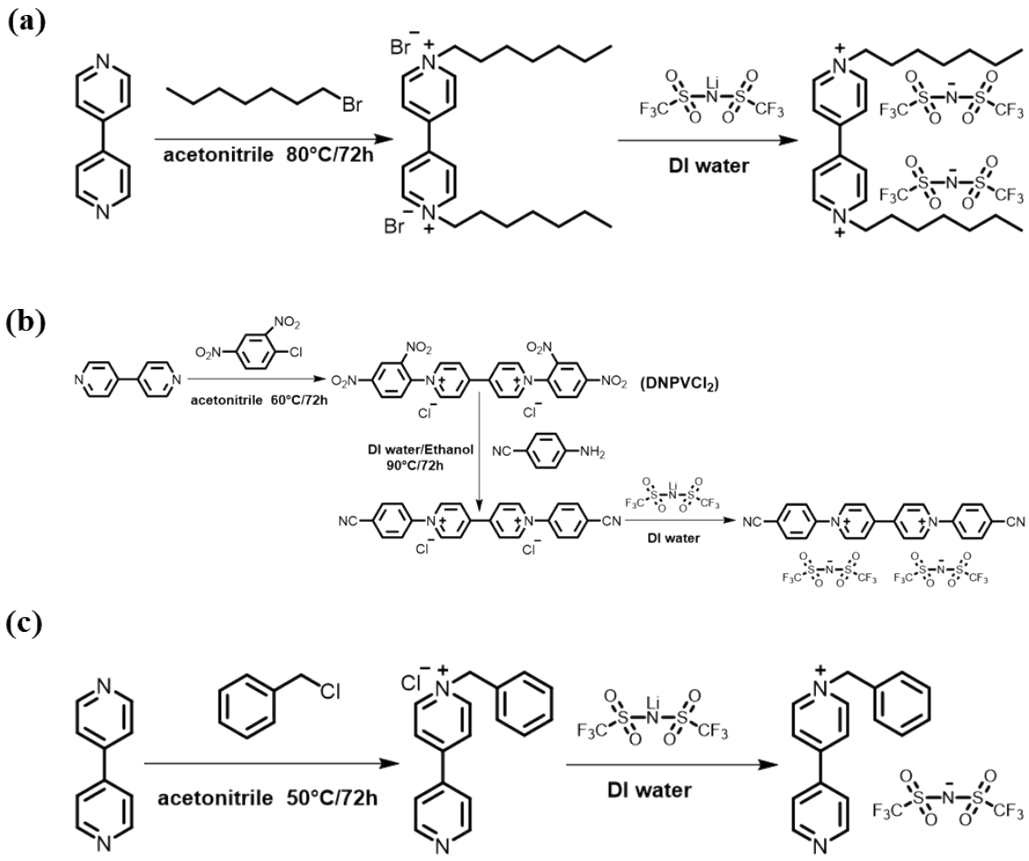

Figure S1. Synthesis of viologens: (a)DHV[TFSI]$_2$, (b)CNPV[TFSI]$_2$, (c)MBV[TFSI].

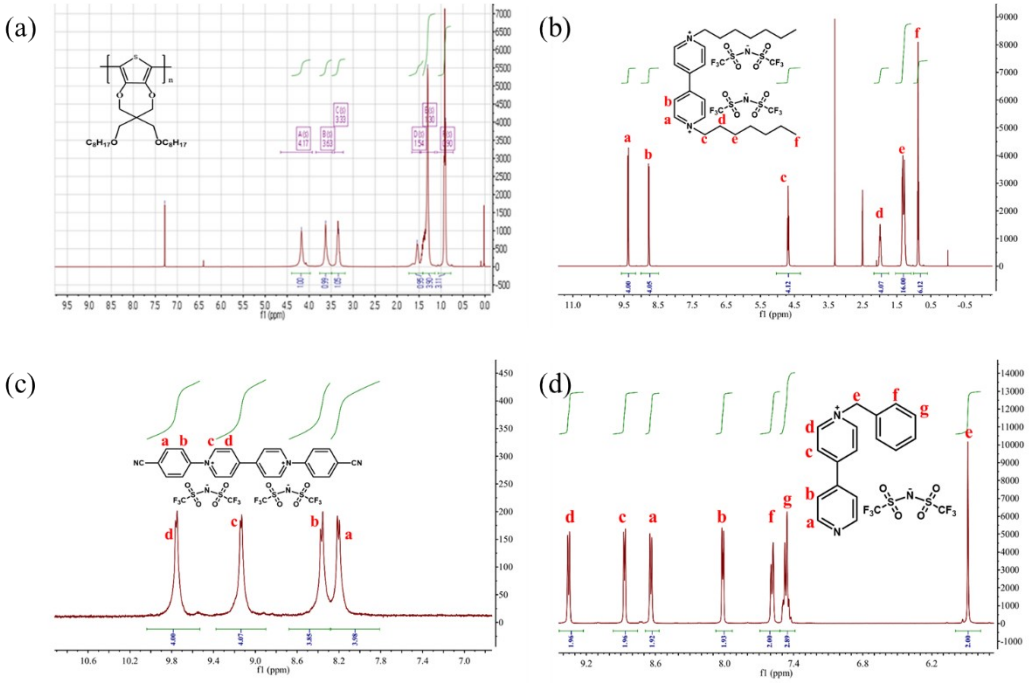

Figure S2. The ^{1}H NMR spectra of the (a)PProDOT-C8 (400 MHz, 25 °C, $CDCl_3$), (b)

DHV[TFSI]$_2$ (400 MHz, 25 °C, DMSO-d_6), (c)CNPV[TFSI]$_2$ (400 MHz, 25 °C, DMSO-d_6), (d)MBV[TFSI] (400 MHz, 25 °C, DMSO-d_6).

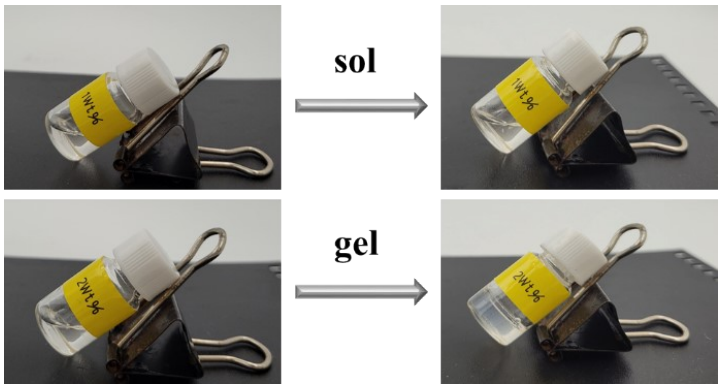

Figure S3. Gel test of 1wt% and 2wt% DBS

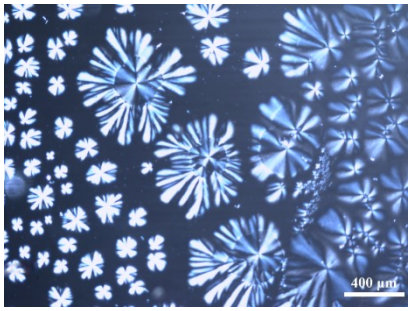

Figure S4. The polarizing microscope image of DBS-G

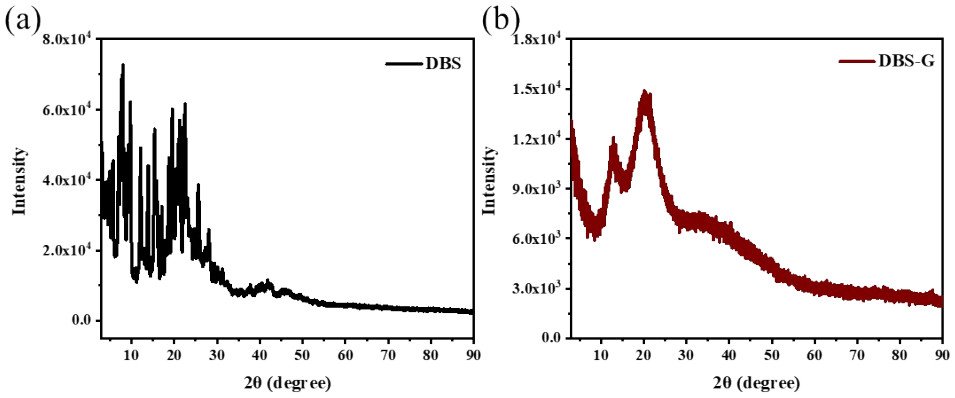

Figure S5. XRD diffractogram of the (a)DBS, (b)DBS-G.

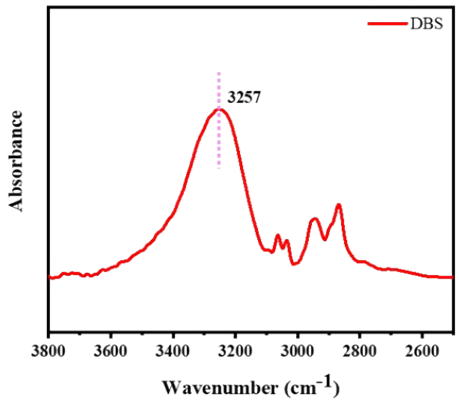

Figure S6. The Fourier transform infrared spectrum of DBS

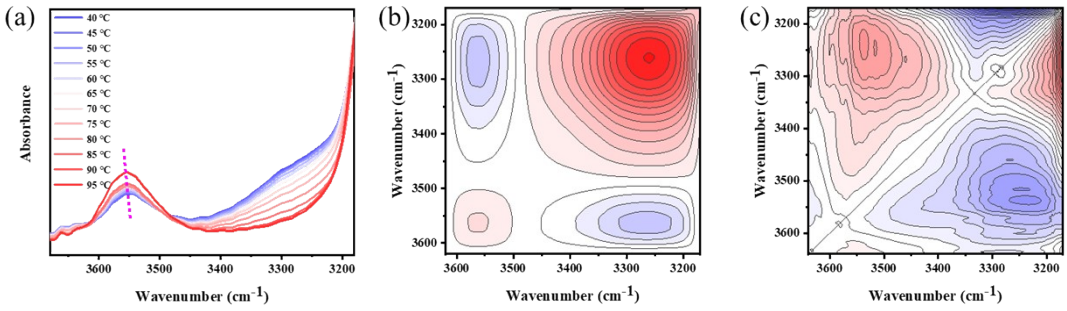

Figure S7. (a) Fourier transform infrared spectra of DBS, [BMIm][TFSI], and DBS-G. (b) 2D infrared correlation synchronous spectrum of DBS-G. (c) 2D infrared correlation asynchronous spectrum of DBS-G.

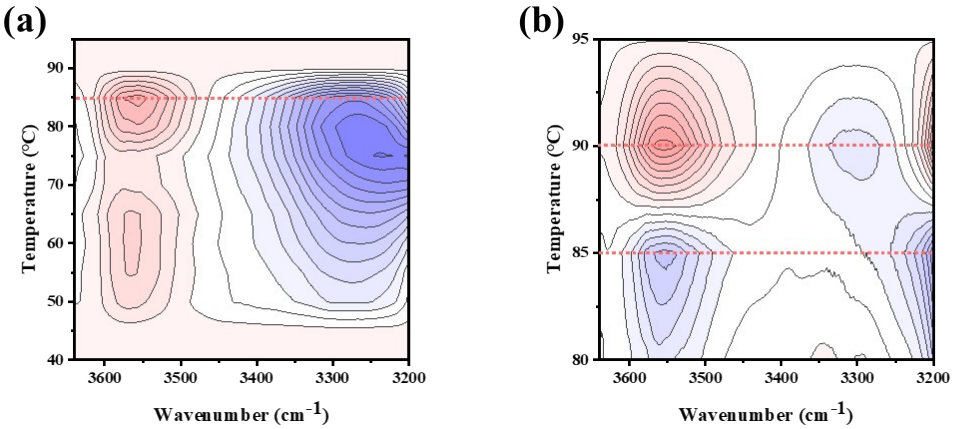

Figure S8. (a) PCMW synchronous infrared spectrum of DBS-G. (b) PCMW asynchronous infrared spectrum of DBS-G.

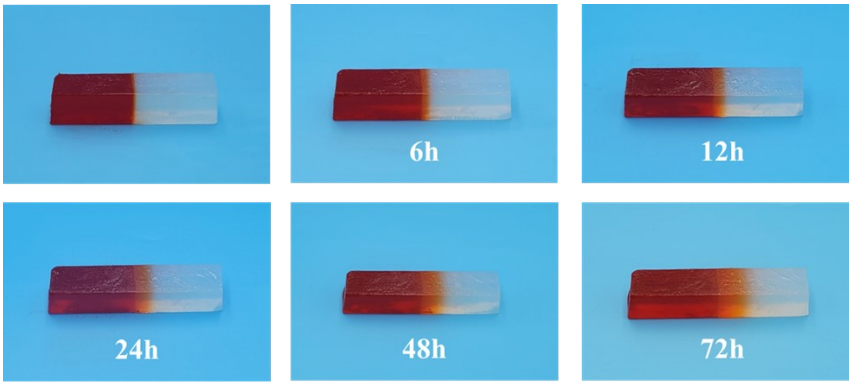

Figure S9. In the self-healing experiment of DBS-G, the red part was dyed with 0.1wt% Sudan red.

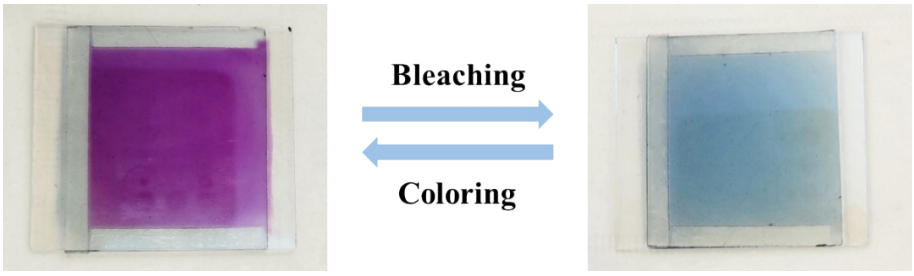

Figure S10. The coloring and bleaching state of PProDOT-C8-ECD

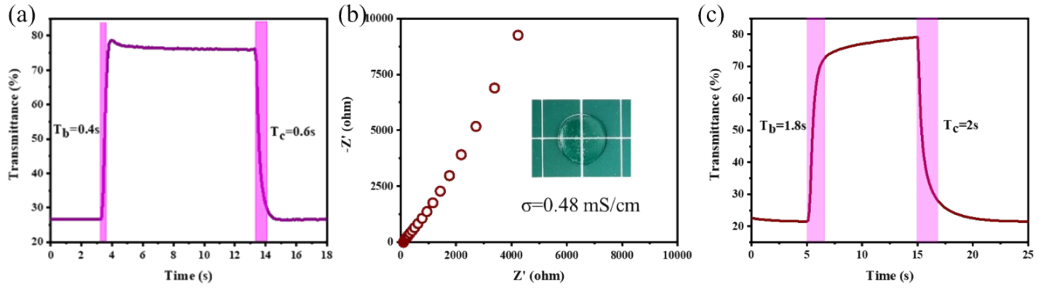

Figure S11. UV-vis kinetic spectrum of the PProDOT-C8-ECD using the electrolyte of [BMIm][THSI], (b) Electrochemical impedance spectroscopy of MEA-G(The illustration is a photo of MEA-G). (c) UV-vis kinetic spectrum of the PProDOT-C8-ECD using the electrolyte of MEA-G.

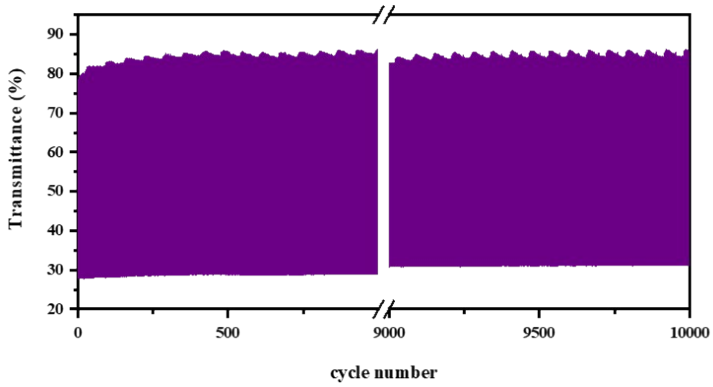

Figure S12. The 10,000 cycle stability test of PProDOT-C8-ECD, applying the voltage of 0.8 V and -0.8 V circularly.

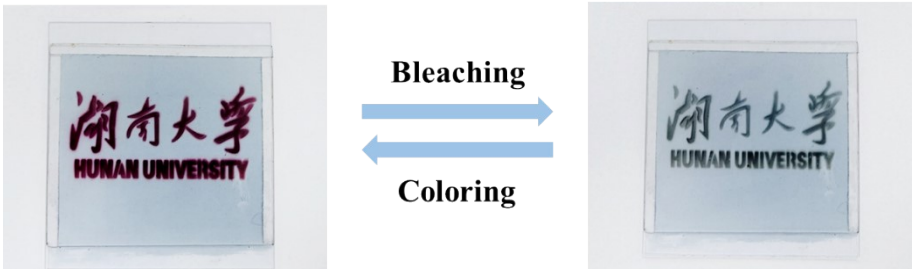

Figure S13. The coloring and bleaching process of the PProDOT-C8-ECD pattern

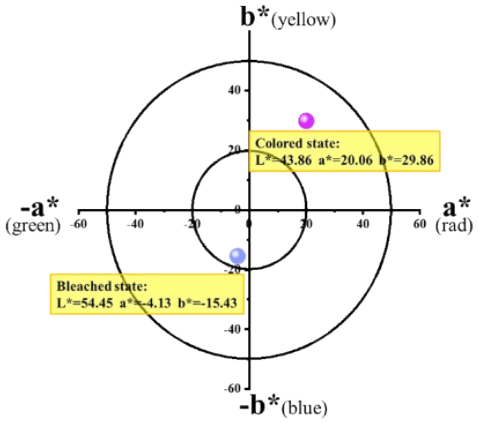

Figure S14. CIE L*a*b* values of the coloring and bleaching states in the PProDOT-C8- ECD

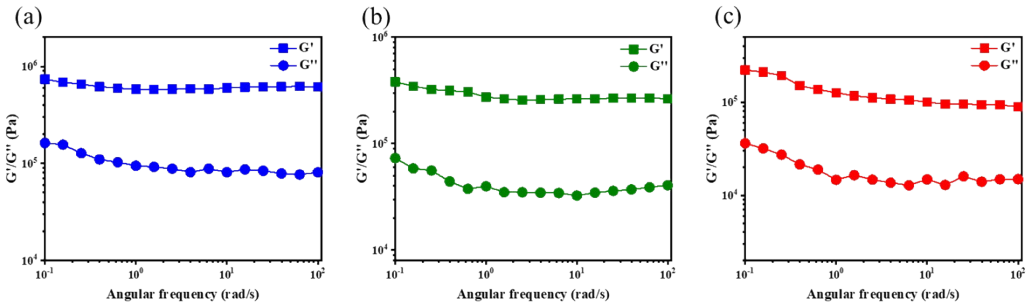

Figure S15. The rheological test of (a)DHV[TFSI]$_2$-G, (b)CNPV[TFSI]$_2$-G, (c)MBV[TFSI]-G (strain=1%).

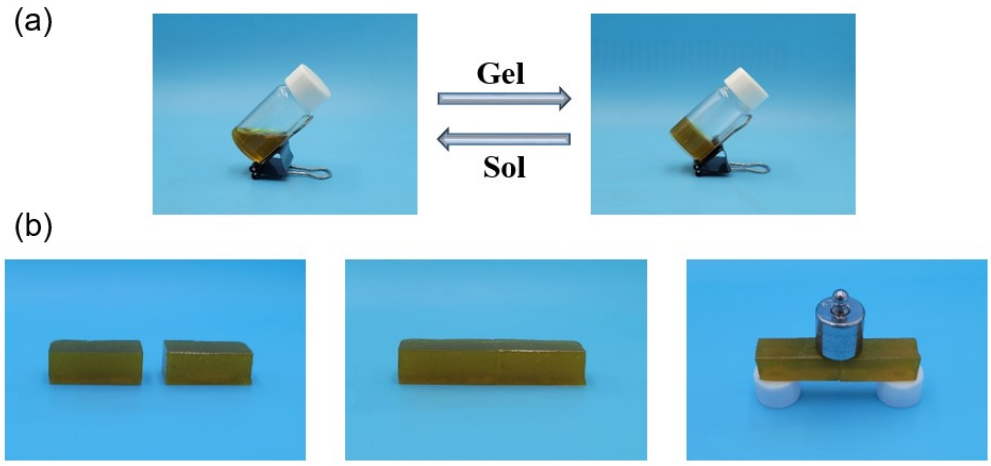

Figure S16. (a) Gelation and solation processes of viologen-containing EC gel. (b) Self-healing process of viologen-containing EC gel.

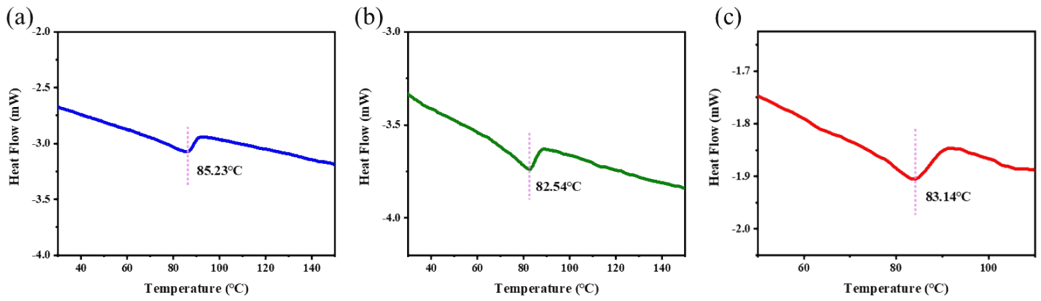

Figure S17. The differential scanning calorimetry (DSC) curve of (a) DHV[TFSI]$_2$-G, (b)CNPV[TFSI]$_2$-G, (c)MBV[TFSI]-G.

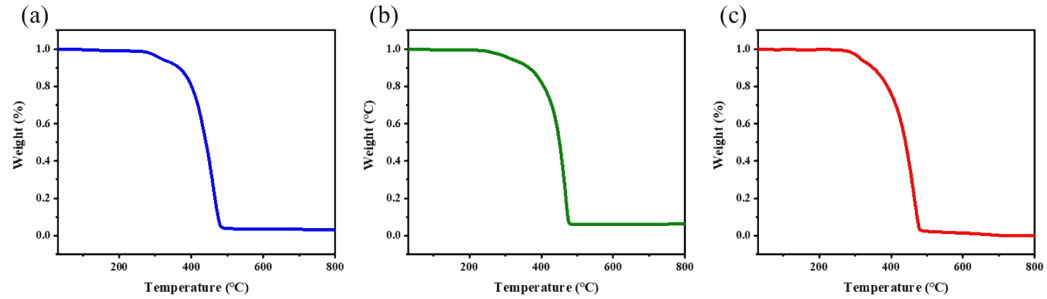

Figure S18. The thermogravimetric curve of (a) DHV[TFSI]$_2$-G, (b)CNPV[TFSI]$_2$-G, (c)MBV[TFSI]-G.

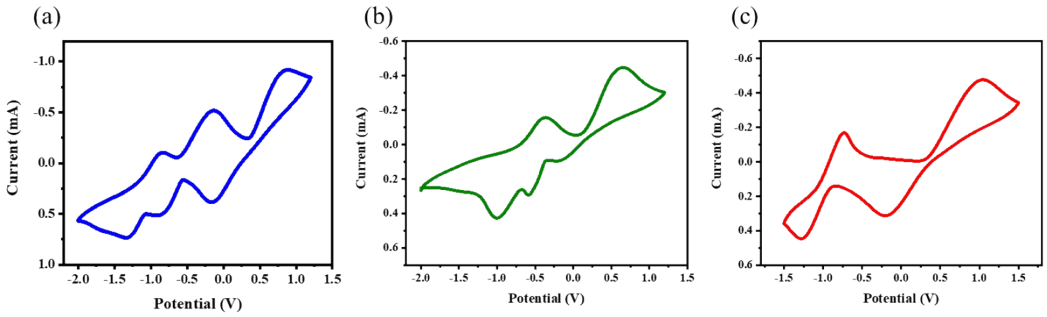

Figure S19. The CVs of the EC gel of (a) DHV[TFSI]$_2$-G, (b)CNPV[TFSI]$_2$-G, (c)MBV[TFSI]-G. The scanning rate is 100 mv/s, with ITO-coated glass as the working electrode, platinum wire as the counter electrode, and silver wire as the reference electrode.

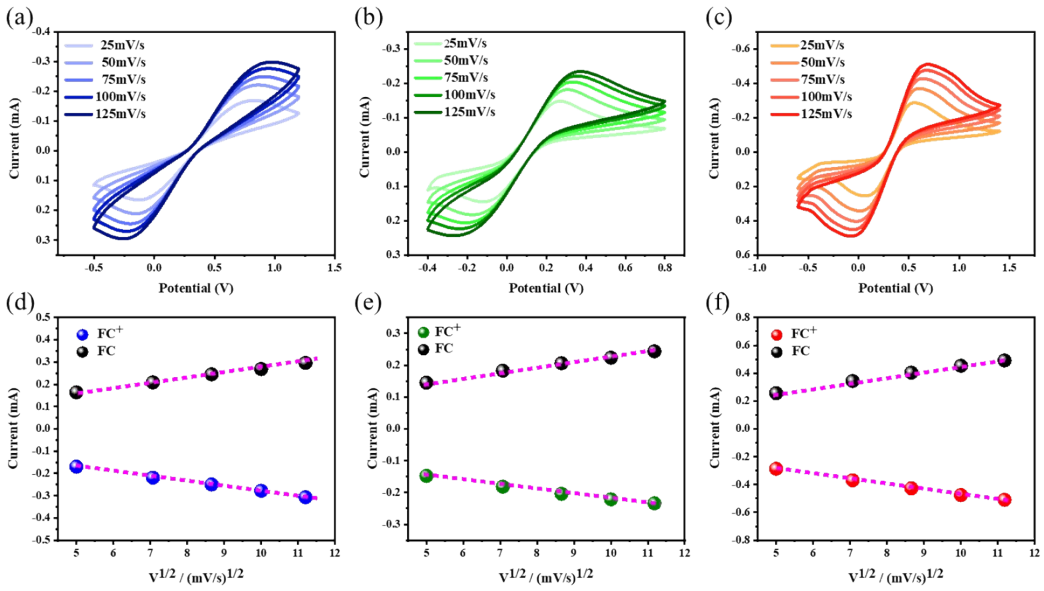

Figure S20. CVs of (a)DHV[TFSI]$_2$-G, (b)CNPV[TFSI]$_2$-G, (c)MBV[TFSI]-G, with varying scan rates of 25, 50, 75, 100, and 125 mV/s. The plots of the anodic and cathodic current peaks (μA) of (d)DHV[TFSI]$_2$-G, (e)CNPV[TFSI]$_2$-G, (f)MBV[TFSI]-G are given as a function of the square root of the scan rate.

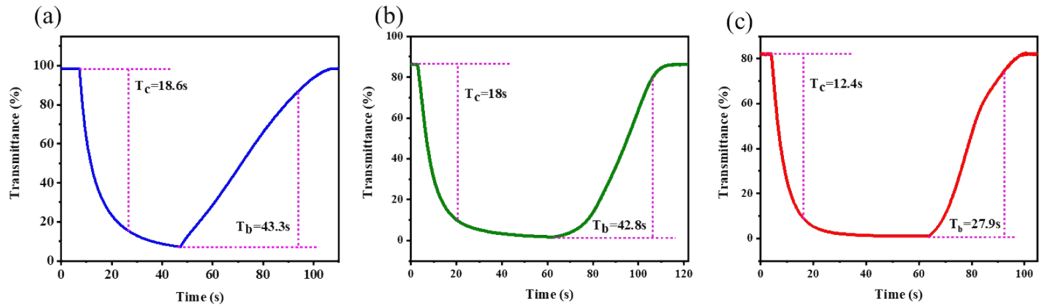

Figure S21. The UV-vis kinetic spectra of the liquid ECD removing the gelator DBS, (a) DHV[TFSI]$_2$-G-ECD, (b)CNPV[TFSI]$_2$-G-ECD, (c)MBV[TFSI]-G-ECD. The test wavelength was fixed at 607, 595, and 374 nm, and the voltage at -1.2, -0.8, and -1.5 V respectively.

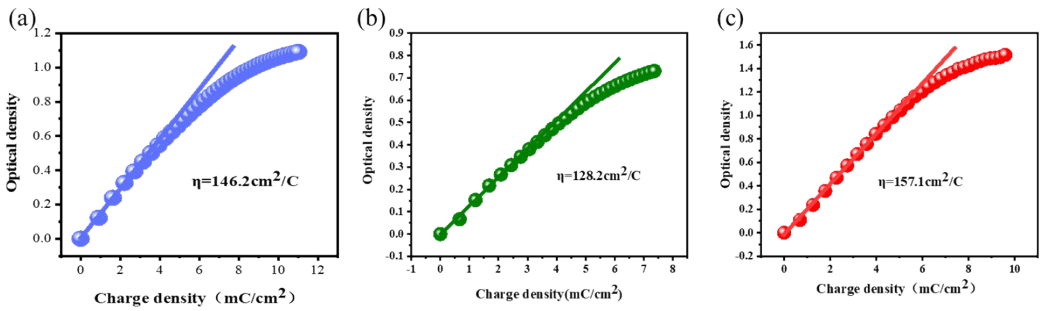

Figure S22. The coloring efficiency of the (a)DHV[TFSI]$_2$-G-ECD, (b)CNPV[TFSI]$_2$-G-ECD, and (c)MBV[TFSI]-G. The coloration efficiency was estimated from a fitted slope in the linear regime of each plot.

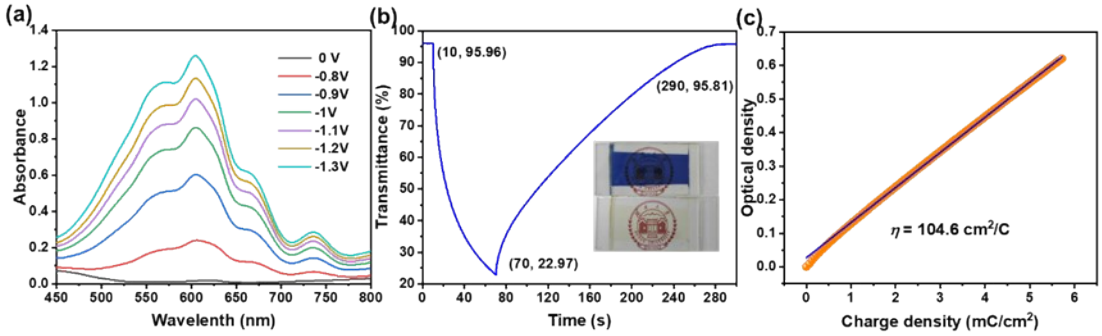

Figure S23. (a) UV-Vis absorption spectra of DHV[TFSI]$_2$-PMMA-G-ECD measured at the same voltages as those applied to DHV[TFSI]$_2$-DBS-G-ECD; (b) Kinetic UV-Vis spectrum of DHV[TFSI]$_2$-PMMA-G-ECD at a test wavelength of 607 nm, featuring periodic voltage variations between 0 V and -1.2 V (inset: comparison of DHV[TFSI]$_2$-PMMA-G-ECD before and after electrochromism); (c) Coloring efficiency of DHV[TFSI]$_2$-PMMA-G-ECD.

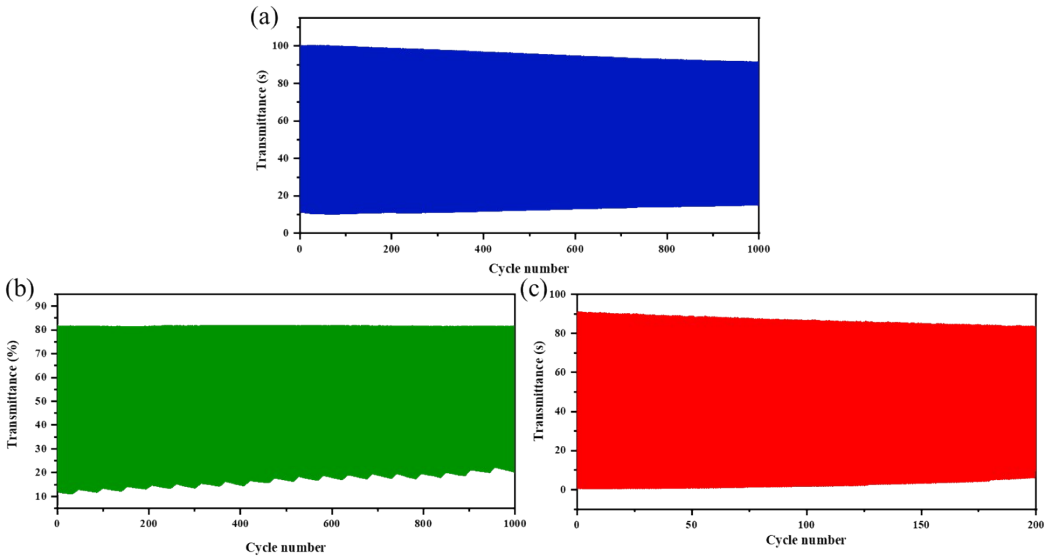

Figure S24. Cyclic stability test of of (a) DHV[TFSI]$_2$-G-ECD, (b)CNPV[TFSI]$_2$-G-ECD, (c)MBV[TFSI]-G-ECD.

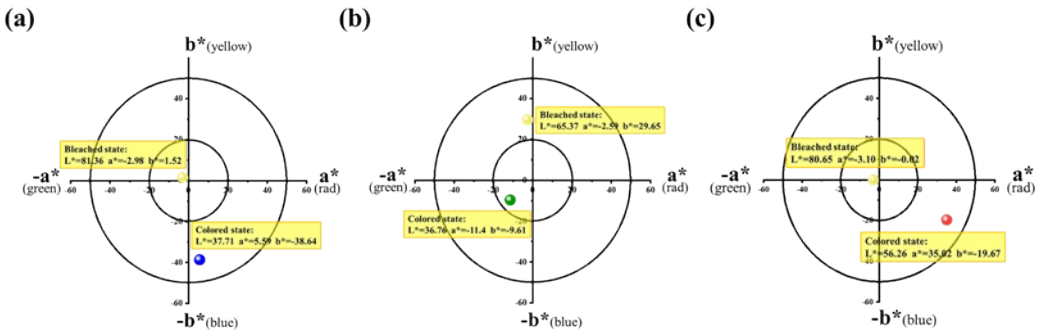

Figure S25. CIE L*a*b* values of the bleaching and coloring states of the (a) DHV[TFSI]$_2$-G-ECD, (b) CNPV[TFSI]$_2$-G-ECD, (c) MBV[TFSI]-G-ECD.

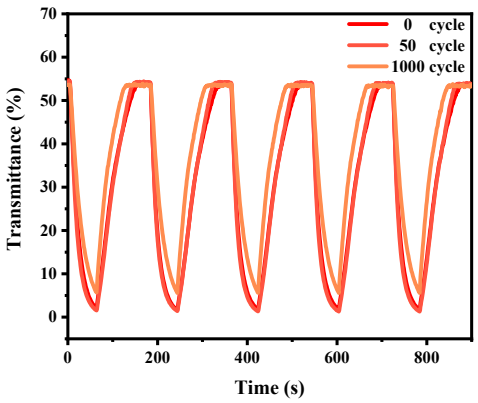

Figure S26. The UV-vis kinetic spectrum of the flexible ECD at bending cycles of 0, 50, and 1000 respectively.

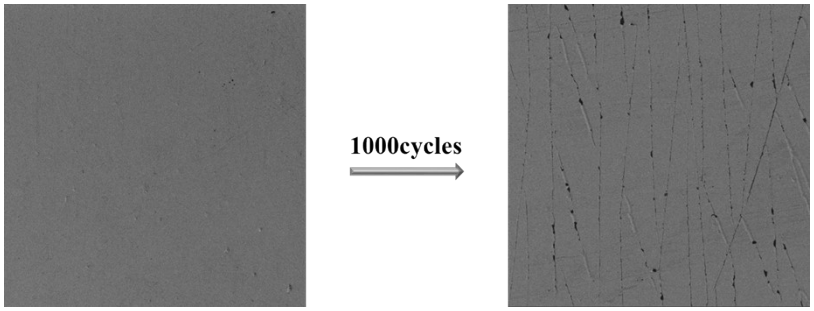

Figure S27. Scanning electron microscope (SEM) images of ITO-coated PET film after 1000 bending cycles.

Table S1. Performance comparison of this work with various polymer-based ECDs.

EC materials	ΔT (%)	t_c (s)	t_b (s)	η (cm^2/C)	Refs
PProDOT-C8	49	0.6	0.9	1070	This Work
PV1	68	10	25	102.8	[1]
AP-ViO-PIL	62	29	11	112	[2]
ProDOT-Et2	59	70.6	11.3	1214	[3]
PDBF-3HexTh	32.8	4.6	6.6	372	[4]
PCET	79	1.5	7	1240	[5]
P(DT-TP)	50	9.5	0.4	1323	[6]
PEDOT:PSS	25.4	5.3	1.8	143	[7]
Viologen 2D Polymer	21	2.8	1.2	989	[8]
Poly[Ni(3- Mesalen)]	32.7	13	10	152	[9]
RHMA-M1	70	1.5	7	1240	[10]

* The response speed, defined as the time required for coloring and bleaching to reach 90% of the maximum transmittance.

Table S2. Performance comparison of this work with various viologen-based ECDs

EC materials	ΔT (%)	T_c (s)	T_b (s)	η (cm^2/C)	Refs
$DHV[TFSI]_2$	91	21	48	146.2	This work
$CNPV[TFSI]_2$	78	29.8	52.7	128.2	
MBV[TFSI]	82	17.9	31.7	157.1	
TEG-[C_4C_3bpy]TFSI	10.1	72	51	36.1	11
TEG-[C_6C_3bpy]TFSI	21.6	14	17	76.8	
HEG-[C_6C_3bpy]TFSI	18.1	59	19	12.27	
$CF_3PhV[PF_6]_2$	~95	40	180	81	12
$DHV[PF_6]_2$	~95	11	280	78	
$CNPhV[PF_6]_2$	~95	18	300	155	
$CF_3PhV[PF_6]_2$	~90	71	253	140	13
$EtV[PF_6]_2$	~90	58	86	131	
$CF_3FPhV[PF_6]_2$	~90	80	108	87	
$MHV[PF_6]_2$	over 90%	19	31	80.7	14
$DHV[PF_6]_2$	over 90%	20	34	87.3	
$DHV[PF_6]_2$ &$DPV[PF_6]_2$	over 90%	39	21	54.6	
MHV-H	65	56	36	94.5	15
$2TPAV^{2+}[PF_6]_2$	16.4	93	95	16	16
$2PPV^{2+}[PF_6]_2$	51.4	100	90	69	
$2PCV^{2+}[PF_6]_2$	62.1	28	30	137	
$[HERFV][PF_6]_2$	35.4	15	22	107.3	17

$[HERFV][TFSI]_2$	56	15	42	120.33	
$Fc/HV[BF_4]^2$	58.9	1.80	1.56	31.7	
$Fc/OV[BF_4]^2$	57.1	2.31	1.72	35.1	[18]
$Fc/NV[BF_4]^2$	56.7	1.95	1.81	36.2	
BnPyV	68	38	27	35.40	
OCF3- BnPyV	85	31	39	140.17	[19]
OCH3- BnPyV	70	18	30	99.59	
3,4,5-OCH3-BnPyV	72	29	49	108.29	

* The response speed, defined as the time required for coloring and bleaching to reach 90% of the maximum transmittance.

References

1. Y. Zhang, X. Jin, W. Zhang, C. Gu, X. Liu and Y.-M. Zhang, *Dyes Pigm.*, 2023, **209**, 110902.
2. X. Wu, Q. Fan, Z. Bai, Q. Zhang, W. Jiang, Y. Li, C. Hou, K. Li and H. Wang, *Small*, 2023, **19**, n/a-n/a.
3. K.-C. Chen, C.-Y. Hsu, C.-W. Hu and K.-C. Ho, *Sol. Energy Mater. Sol. Cells*, 2011, **95**, 2238-2245.
4. K. Lin, S. Ming, S. Zhen, Y. Zhao, B. Lu and J. Xu, *Polym. Chem.*, 2015, **6**, 4575-4587.
5. Y. Wang, S. Wang, X. Wang, W. Zhang, W. Zheng, Y.-M. Zhang and S. X.-A. Zhang, *Nat. Mater.*, 2019, **18**, 1335-1342.
6. J. Kim, Y. R. In, T. N.-L. Phan, Y. M. Kim, J.-W. Ha, S. C. Yoon, B. J. Kim and H. C. Moon, *Chem. Mater.*, 2023, **35**, 792-800.
7. C. Preston, Y. Dobashi, N. T. Nguyen, M. S. Sarwar, D. Jun, C. Plesse, X. Sallenave, F. Vidal, P.-H. Aubert and J. D. W. Madden, *ACS Appl. Mater. Interfaces*, 2023, **15**, 28288-28299.
8. Z. Wang, X. Jia, P. Zhang, Y. Liu, H. Qi, P. Zhang, U. Kaiser, S. Reineke, R. Dong and X. Feng, *Adv. Mater*., 2022, **34**, 2106073.
9. M. Nunes, M. Araújo, J. Fonseca, C. Moura, R. Hillman and C. Freire, *ACS Appl. Mater. Interfaces*, 2016, **8**, 14231-14243.
10. Y. Wang, S. Wang, X. Wang, W. Zhang, W. Zheng, Y. M. Zhang and X. A. Zhang, *Nature Mater.*, 2019, **18**, 1335-1342.
11. J. M. C. Puguan and H. Kim, *J. Mater. Chem. A*, 2019, **7**, 21668-21673.
12. H. C. Moon, C. H. Kim, T. P. Lodge and C. D. Frisbie, *ACS Appl. Mater. Interfaces*, 2016, **8**, 6252-6260.
13. H. Oh, J. K. Lee, Y. M. Kim, T. Y. Yun, U. Jeong and H. C. Moon, *ACS Appl. Mater. Interfaces*, 2019, **11**, 45959-45968.
14. J. W. Kim and J. M. Myoung, *Adv. Funct. Mater.*, 2019, **29**, 1808911.
15. T. Y. Yun and H. C. Moon, *Org. Electron.*, 2018, **56**, 178-185.
16. M. Zhu, J. Zeng, H. Li, X. Zhang and P. Liu, *Synth. Met.*, 2020, **270**, 116579.
17. G. K. Pande, N. Kim, J. H. Choi, G. Balamurugan, H. C. Moon and J. S. Park, *Sol. Energy Mater. Sol. Cells*, 2019, **197**, 25-31.
18. H. C. Lu, S. Y. Kao, H. F. Yu, T. H. Chang, C. W. Kung and K. C. Ho, *ACS Appl. Mater. Interfaces*, 2016, **8**, 30351-30361.
19. B. Deng, Y. Zhu, M. U. Ali, K. Li, X. Liu, X. Zhang, J. Ning, Z. Hu, H. Chen, J. He, Y. He and H. Meng, *Sol. Energy Mater. Sol. Cells*, 2023, **251**, 112149.